

Anisotropic spin fluctuations in the triangular Kondo lattice compound $\text{CePtAl}_4\text{Ge}_2$ probed by site-selective ^{27}Al NMR

H. Sakai,^{1,*} S. Shin,^{2,3} S. Kambe,¹ Y. Tokunaga,¹ H. Harima,⁴ E. Pomjakushina,² and T. Park³

¹*Advanced Science Research Center, Japan Atomic Energy Agency, Tokai, Ibaraki 319-1195, Japan*

²*PSI Center for Neutron and Muon Sciences, Paul Scherrer Institut, 5232 Villigen PSI, Switzerland.*

³*Center for Quantum Materials and Superconductivity (CQMS) and Department of Physics, Sungkyunkwan University, Suwon 16419, South Korea.[†]*

⁴*Graduate School of Science, Kobe University, Kobe 657-8501, Japan*

(Dated: September 4, 2025)

A site-selective ^{27}Al nuclear magnetic resonance (NMR) study is carried out on the Kondo lattice compound $\text{CePtAl}_4\text{Ge}_2$, which crystallizes in a rhombohedral lattice with quasi-two-dimensional Ce layers forming a triangular lattice network. Two inequivalent Al sites, Al(1) and Al(2), are unambiguously assigned by comparing measured nuclear quadrupole parameters with electric field gradients obtained from electronic structure calculations. Knight shift analysis yields distinct hyperfine coupling constants, revealing that they arise predominantly from RKKY-type transferred hyperfine fields through conduction electrons. Spin-lattice relaxation measurements reveal pronounced anisotropic spin fluctuations, and comparison of the relaxation rates between the two Al sites clarifies the momentum-space structure of these fluctuations. At low magnetic fields, $(T_1T)^{-1}$ is strongly enhanced on cooling toward the Néel temperature, indicating the growth of in-plane antiferromagnetic correlations in the paramagnetic state.

I. INTRODUCTION

Frustrated magnetism in f -electron Kondo systems offers fertile ground for unconventional spin states, where the competition between Ruderman–Kittel–Kasuya–Yosida (RKKY) interactions and Kondo screening is strongly shaped by lattice geometry [1–4]. Indeed, in Kondo lattice compounds where rare-earth or actinide ions form geometrically frustrated networks, such frustration can stabilize partial magnetic order and complex spin textures that are absent in conventional Kondo lattice compounds. Yet, a detailed microscopic understanding of their spin dynamics remains limited, particularly regarding how geometrical frustration influences low-energy spin fluctuations in the presence of anisotropic interactions.

Representative examples such as CePdAl [5–8] and UNi_4B [9–11] feature quasi-kagome or distorted triangular lattice networks. In these compounds, partial magnetic order emerges as a consequence of selective Kondo screening within geometrically constrained networks. Such behavior illustrates how magnetic frustration can suppress conventional long-range order and give rise to exotic spin textures in f -electron systems.

In contrast, trigonal $\text{CePtAl}_4\text{Ge}_2$ hosts a triangular lattice network of Ce ions stacked along the c axis [12], providing a structurally simpler platform to explore frustrated Kondo magnetism without site disorder. Neutron diffraction has revealed a longitudinal spin-amplitude-modulated magnetic structure in this compound below

$T_N = 2.3$ K [13, 14], positioning it as a rare system where frustration, Kondo coherence, and magnetic anisotropy interplay in a clean setting. Compositional relatives such as the tetragonal $\text{CeMAl}_4\text{Si}_2$ family ($M = \text{Rh, Ir, Pt}$), where Ce ions form square lattices, lack geometrical frustration but exhibit a range of magnetic ground states from antiferromagnetic to ferromagnetic [15, 16]. Among them, $\text{CeRhAl}_4\text{Si}_2$ has been studied using ^{27}Al NMR, revealing anisotropic spin fluctuations associated with Fermi surface nesting [17], and illustrating the power of site-selective NMR in probing low-energy spin dynamics.

In this work, a ^{27}Al NMR study on single-crystalline $\text{CePtAl}_4\text{Ge}_2$ is presented to investigate its local magnetic properties and spin fluctuations under geometrical frustration. By assigning the two inequivalent Al sites using electric field gradients (EFGs) obtained from electronic structure calculations, site-resolved Knight shift and spin-lattice relaxation measurements are carried out. The results reveal highly anisotropic, predominantly in-plane spin fluctuations and their suppression under magnetic fields, offering microscopic insights into frustration-driven spin dynamics in a triangular f -electron system.

II. EXPERIMENTAL DETAILS

Single crystals of $\text{CePtAl}_4\text{Ge}_2$ were grown using a self-flux method with an $\text{Al}_{0.73}\text{Ge}_{0.27}$ mixture, as described in Ref. 12. X-ray diffraction confirmed the rhombohedral lattice and single-phase quality of the crystals. The chemical composition was verified using energy-dispersive X-ray spectroscopy. For NMR measurements, a single crystal was mounted on a glass slip and tightly wound with copper wire to form a radio-frequency (rf) coil. This coil was placed in a standard ^4He cryostat equipped with a superconducting magnet and a variable-

* sakai.hironori@jaea.go.jp

[†] Current affiliation: Jülich Centre for Neutron Science (JCNS) at the Heinz Maier-Leibnitz Zentrum (MLZ), Forschungszentrum Jülich GmbH, Lichtenbergstraße 1, 85747, Garching, Germany.

temperature insert. A dual-axis goniometer enabled in-situ rotation of the sample with respect to the external magnetic field. For measurements at temperatures between approximately 100 mK and 2 K, a ^3He – ^4He dilution refrigerator was used without the goniometer. ^{27}Al NMR (nuclear spin $I = 5/2$) spectra were acquired using a spin-echo technique with a phase-coherent pulsed NMR spectrometer. The spectra were constructed using Fourier transforms of the spin-echo signals collected over a range of carrier frequencies. The nuclear quadrupole frequency is defined as $\nu_Q \equiv |3e^2qQ/2I(2I-1)\hbar|$, where eQ is the nuclear quadrupole moment and $eq \equiv V_{ZZ}$ is the largest principal component of the EFG tensor. The principal components of the EFG (V_{ii}) satisfy $|V_{XX}| \leq |V_{YY}| \leq |V_{ZZ}|$ and $V_{XX} + V_{YY} + V_{ZZ} = 0$. The asymmetry parameter is defined as $\eta \equiv |V_{YY} - V_{XX}|/|V_{ZZ}|$. We used the nuclear quadrupole moment for ^{27}Al of $^{27}Q = 0.1466 \times 10^{-28} \text{ m}^2$ [18] and the nuclear gyromagnetic ratio $^{27}\gamma_n/2\pi = 11.094 \text{ MHz/T}$. The nuclear spin-lattice relaxation time T_1 was determined using the inversion-recovery method. Magnetization recovery curves were well fitted by single-component relaxation functions for both the second satellite transitions: $\{M(\infty) - M(t)\}/M(\infty) = \frac{1}{35}e^{-t/T_1} + \frac{3}{14}e^{-3t/T_1} + \frac{2}{5}e^{-6t/T_1} + \frac{2}{7}e^{-10t/T_1} + \frac{1}{14}e^{-15t/T_1}$, corresponding to the expected relaxation functions for spin $I = 5/2$ nuclei under magnetic relaxation.

III. RESULTS AND DISCUSSIONS

A. ^{27}Al NMR spectra and site-specific assignments

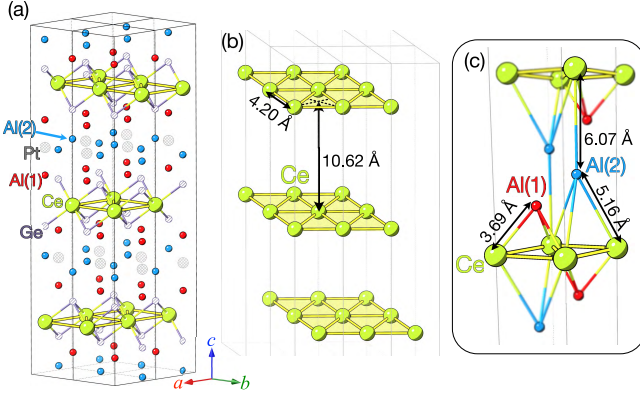


FIG. 1. (a) Crystal structure of $\text{CePtAl}_4\text{Ge}_2$, consisting of alternating Ce layers and PtAl_4Ge_2 slabs stacked along the c axis. (b) Extracted Ce sublattice highlighting the two-dimensional triangular lattice network. (c) Local environments of the two inequivalent Al sites, Al(1) and Al(2). Pt and Ge atoms are omitted for clarity.

To interpret the ^{27}Al NMR spectra in $\text{CePtAl}_4\text{Ge}_2$, it is essential to understand its crystal structure and the local environments of the Al sites, which determine the hy-

perfine and quadrupolar interactions. $\text{CePtAl}_4\text{Ge}_2$ crystallizes in the $\text{YNiAl}_4\text{Ge}_2$ -type structure with a rhombohedral lattice (space group $R\bar{3}m$, No.166), as illustrated in Fig.1(a) [12]. The structure consists of alternating Ce layers and PtAl_4Ge_2 slabs stacked along the c axis, with lattice parameters $a = 4.1995\text{\AA}$ and $c = 31.851\text{\AA}$. The Ce atoms form a well-separated triangular-lattice network, giving rise to a two-dimensional frustrated geometry [Fig. 1(b)]. Two inequivalent Al sites, Al(1) and Al(2), both occupy Wyckoff $6c$ positions with local $3m$ symmetry, as shown in Fig.1(c).

Figure 2(a) shows the ^{27}Al NMR spectra recorded at 20 K under $\mu_0 H_0 = 2.8993 \text{ T}$ for both $H_0 \parallel a$ and $H_0 \parallel c$. Each spectrum contains five quadrupole-split lines from the $I = 5/2$ nuclei at the Al(1) and Al(2) sites. No additional splitting is observed upon rotation, indicating that each site maintains equivalent local symmetry under the field.

Both Al sites share the same axial $3m$ symmetry, ensuring that the EFG tensor is axially symmetric with asymmetry parameter $\eta = 0$. This is consistent with the observed angular dependence: satellite splitting is maximized for $H_0 \parallel c$, and no in-plane anisotropy is seen under azimuthal rotation, as shown in Fig. 2(c). These features confirm that the EFG principal axis is aligned along the c axis at both sites.

The observed spectra are reproduced by numerically diagonalizing the nuclear spin Hamiltonian $\mathcal{H} = \mathcal{H}_Z + \mathcal{H}_Q$, where

$$\mathcal{H}_Z = \gamma_n \hbar \{1 + K(\Theta)\} \mathbf{I} \cdot \mathbf{H}_0, \quad (1)$$

and

$$\mathcal{H}_Q = \frac{\hbar \nu_Q}{6} (3I_z^2 - I(I+1)). \quad (2)$$

Assuming axial anisotropy in the Knight shift, the angle-dependent shift is modeled as $K(\Theta) = K_c \cos^2 \Theta + K_a \sin^2 \Theta$, where K_a and K_c denote the Knight shifts along the a and c axes. The parameters K_a , K_c , and ν_Q are optimized to fit the observed angular dependence of the resonance frequencies.

The best-fit parameters are $\nu_Q = 1.23 \pm 0.01 \text{ MHz}$, $K_a = 0.665 \pm 0.001\%$, and $K_c = -0.04 \pm 0.01\%$ for the Al(1) site, and $\nu_Q = 1.47 \pm 0.01 \text{ MHz}$, $K_a = -0.031 \pm 0.001\%$, and $K_c = 0.20 \pm 0.01\%$ for the Al(2) site. Since both sites share the same local symmetry, these values alone do not uniquely determine the site assignment. To resolve this ambiguity, nuclear quadrupole frequencies are compared with calculated values ν_Q^{calc} . The ν_Q^{calc} is obtained from the electronic structure calculations using the full-potential linearized augmented plane wave (FLAPW) method based on the local density approximation (LDA), with the procedure of Blaha *et al.* [19]. This approach has proven reliable in various Ce-based intermetallics, including $\text{CeRu}_2\text{Al}_{10}$ [20], $\text{CeRu}_2\text{Al}_2\text{B}$ [21], $\text{CeRu}_2\text{Ga}_2\text{B}$ [22], and $\text{CeRhAl}_4\text{Si}_2$ [17]. For $\text{LaPtAl}_4\text{Ge}_2$ and $\text{CePtAl}_4\text{Ge}_2$, the calculated ν_Q^{calc} values at the Al(1) and Al(2) sites are summarized in Table I. For both

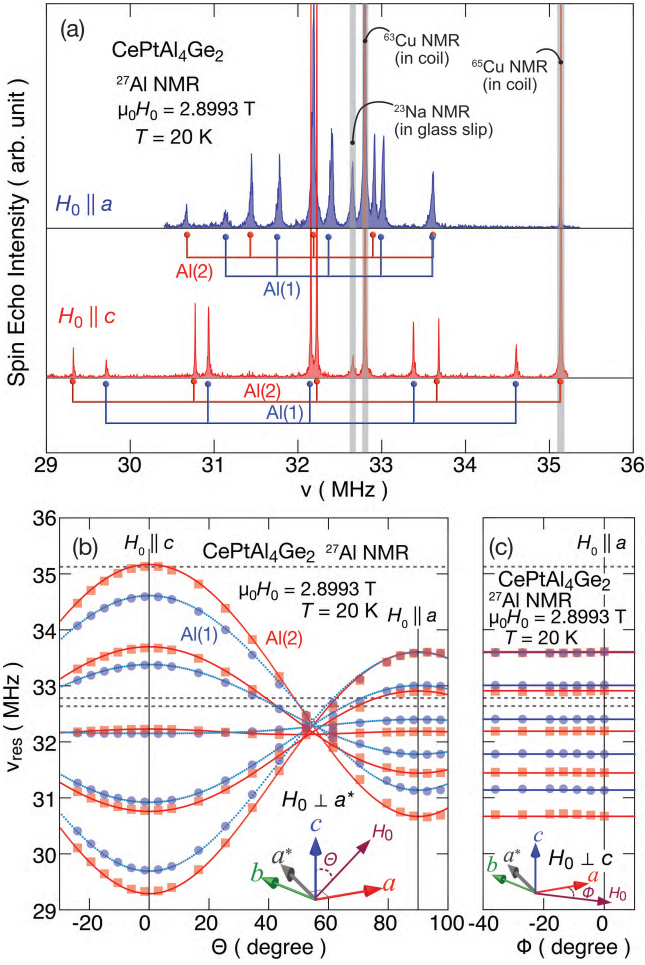


FIG. 2. ^{27}Al NMR spectra of $\text{CePtAl}_4\text{Ge}_2$ at 20 K under a magnetic field of $\mu_0 H_0 = 2.8993$ T. (a) Field-swept spectra measured with $H_0 \parallel a$ and $H_0 \parallel c$. The two sets of lines are assigned to the Al(1) and Al(2) sites based on comparisons with electric field gradient parameters estimated from band structure calculations. Gray shaded regions indicate spectral blind spots due to $^{63,65}\text{Cu}$ NMR signals from the NMR coil and ^{23}Na NMR signals from the glass strip used to mount the crystal. (b) Polar-angle (Θ) dependence of the resonance frequencies for H_0 rotated within the ac plane. Blue circles and red squares represent experimental data, while the bold blue dashed and red solid lines are simulations for the Al(1) and Al(2) sites, respectively, obtained by exact diagonalization of the nuclear spin Hamiltonian. Horizontal dashed lines mark the positions of extrinsic $^{63,65}\text{Cu}$ and ^{23}Na NMR signals. (c) Azimuthal-angle (Φ) dependence of the resonance frequencies for H_0 rotated within the ab plane ($H_0 \perp c$).

$\text{LaPtAl}_4\text{Ge}_2$ and $\text{CePtAl}_4\text{Ge}_2$, the ν_Q^{calc} at the Al(1) site is consistently smaller than that at the Al(2) site. This lower ν_Q^{calc} value in each compound is in very good agreement with the experimentally observed $\nu_Q^{\text{exp}} = 1.23$ MHz, thereby confirming the assignment of the lower ν_Q^{exp} signal to the Al(1) site. The quadrupole frequency shows negligible temperature dependence below approximately 100 K, which justifies comparison with zero-temperature

theoretical values. Furthermore, the experimental value for the Al(2) site is closer to the Ce-based calculation than to that of the La analogue, indicating a substantial contribution of itinerant f electrons to the EFG. This supports the classification of $\text{CePtAl}_4\text{Ge}_2$ as an itinerant f -electron system, consistent with its Kondo-lattice character. Similar estimations of Ce valence from ν_Q variations, reflecting the itinerancy of the $4f$ electrons, have also been reported for the prototypical heavy-fermion compound CeCu_2Si_2 [23].

B. Knight shifts and hyperfine coupling constants

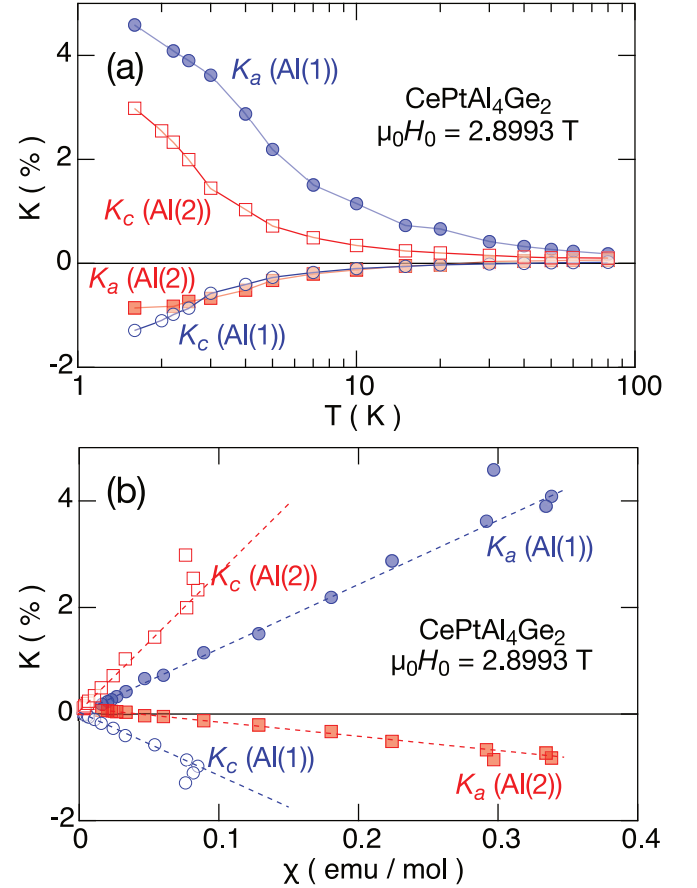


FIG. 3. (a) Temperature dependence of the Knight shifts K_a and K_c for the Al(1) and Al(2) sites in $\text{CePtAl}_4\text{Ge}_2$, measured at $\mu_0 H_0 = 2.8993$ T. (b) Knight shifts plotted against the bulk magnetic susceptibility χ [12], demonstrating linear K - χ relations.

Having established the site assignments of the two inequivalent Al sites, the temperature dependence of the Knight shifts K_a and K_c for Al(1) and Al(2) is obtained, as shown in Fig. 3(a). For the Al(1) site, K_a is positive and K_c is negative, whereas the signs are reversed for the Al(2) site. In all cases, the magnitude of the Knight shift increases monotonically upon cooling, following a Curie-Weiss-like behavior. This indicates that

TABLE I. Summary of the experimental NQR frequency ν_Q^{exp} , calculated values ν_Q^{calc} for LaPtAl₄Ge₂ and CePtAl₄Ge₂, transferred hyperfine coupling constants A_c and A_a (mT/ μ_B), and the shortest Ce–Al bond length $d_{\text{Ce–Al}}$ for the Al(1) and Al(2) sites in CePtAl₄Ge₂.

Site	ν_Q^{exp} (MHz)	ν_Q^{calc} (MHz)		A_c (mT/ μ_B)	A_a (mT/ μ_B)	$d_{\text{Ce–Al}}$ (Å)
		LaPtAl ₄ Ge ₂	CePtAl ₄ Ge ₂			
Al(1)	1.23 ± 0.01	1.261	1.278	67 ± 1	-66 ± 1	3.69
Al(2)	1.47 ± 0.01	1.368	1.461	145 ± 3	-14.9 ± 0.3	5.16

the Knight shifts primarily reflect the $4f$ spin susceptibility of Ce, with distinct hyperfine couplings at each site. Bulk magnetic susceptibility measurements [12] also reveal pronounced anisotropy, with $\chi_{ab} > \chi_c$, and show Curie–Weiss behavior down to T_N for χ_{ab} , and above ~ 275 K for χ_c . The effective moment is estimated as $2.5 \mu_B$ in the high temperature range, close to that of a free Ce³⁺ ion. The Weiss temperatures (θ_W) estimated from Curie–Weiss fits in the high temperature range are -102 K for $H \parallel c$ and 38 K for $H \parallel a$. The large magnitude of the Weiss temperature, relative to the Néel temperature, suggests the presence of strong magnetic frustration.

To derive the hyperfine interactions, standard K – χ plots are constructed using bulk magnetic susceptibility data and the Knight shift values for both crystallographic directions, as shown in Fig.3(b). For each Al site, linear relations are observed between the Knight shift and magnetic susceptibility, with the lines extrapolating to the origin. This confirms that the Knight shifts arise from transferred hyperfine fields induced by the localized Ce moments. The slopes of these K – χ plots yield the transferred hyperfine coupling constants A_i along the i -axis ($i = a, c$), summarized in Table I. These values capture the anisotropic coupling between the Ce $4f$ electrons and the nuclear spins at the two distinct Al sites.

Despite the Al(1) site being located closer to the Ce atom than the Al(2) site [see Fig.1(c) and Table I], the hyperfine coupling constants $|A_i|$ are notably larger at the Al(2) site. This counterintuitive result suggests that the transferred hyperfine interaction is not simply determined by the Ce–Al distance (r_i), but is instead dominated by conduction-electron-mediated couplings, consistent with an RKKY-type mechanism, in which the magnitude of the transferred hyperfine field oscillates as a function of r_i . To evaluate the contribution from dipolar interactions, the expected dipolar fields A_i^{dip} were calculated by summing over Ce³⁺ magnetic moments within a sphere of radius ~ 100 Å. For the Al(1) site, the estimates yield $A_a^{\text{dip}} \approx -28$ mT/ μ_B and $A_c^{\text{dip}} \approx 64$ mT/ μ_B , in good agreement with the experimental values. This agreement suggests that the transferred component of RKKY origin is minimal at Al(1). In contrast, the Al(2) site exhibits $A_a^{\text{dip}} \approx -22$ mT/ μ_B and $A_c^{\text{dip}} \approx 50$ mT/ μ_B , which are much smaller than the measured values. This substantial enhancement indicates a strong transferred hyperfine contribution, reflecting pronounced c -axis anisotropy in the hybridization between Ce $4f$ electrons and conduc-

tion states at Al(2).

C. Spin-lattice relaxation rate and spin dynamics in the paramagnetic state

Spin-lattice relaxation rate ($1/T_1$) measurements of the ²⁷Al nuclei were performed to probe the low-energy spin dynamics in CePtAl₄Ge₂ from a local microscopic perspective. The nuclear magnetization recovery curves at all measured temperatures are well described by the fitting functions given in Sec. II, confirming spatially uniform relaxation governed by magnetic fluctuations. In general, the relaxation rate can be expressed as [24]

$$\frac{1}{T_1} = 2 \left(\frac{\gamma_n A_{\perp}}{\gamma_e \hbar} \right)^2 k_B T \sum_{\mathbf{q}} f^2(\mathbf{q}) \frac{\text{Im} \chi_{\perp}(\mathbf{q}, \omega_0)}{\omega_0}, \quad (3)$$

where γ_e is the electronic gyromagnetic ratio, A_{\perp} is the transverse component of the hyperfine coupling constant, $f(\mathbf{q})$ is the hyperfine form factor, $\text{Im} \chi_{\perp}(\mathbf{q}, \omega_0)$ is the imaginary part of the transverse dynamic spin susceptibility of the Ce $4f$ electrons, and ω_0 is the Larmor angular frequency. Since the $\text{Im} \chi_{\perp}$ term reflects magnetic excitations perpendicular to H_0 , the $1/T_1$ measurements selectively probe transverse low-energy spin fluctuations.

Figure 4 shows the temperature dependence of $1/T_1$ for the Al(1) and Al(2) sites under a magnetic field of $\mu_0 H_0 = 2.8993$ T applied along the a and c axes. At this field strength, the AFM order is completely suppressed for both field orientations, and the system remains in the paramagnetic state over the entire temperature range studied (see Fig. 6(a)). Above $T^* \approx 6$ K, $1/T_1$ exhibits only a weak temperature dependence, consistent with the behavior expected for localized Ce $4f$ moments. This characteristic temperature T^* coincides with the Kondo coherence temperature identified from resistivity measurements [12]. Separately, the magnetic contribution to the resistivity, ρ_m , obtained by subtracting the resistivity of LaPtAl₄Ge₂ from that of CePtAl₄Ge₂, exhibits another broad maximum around ~ 120 K. Bulk susceptibility measurements and neutron scattering results [13] further indicate that the crystalline electric field (CEF) ground state is the $|j_z = \pm 1/2\rangle$ Kramers doublet, with the first excited state $|j_z = \pm 3/2\rangle$ lying about 170 K higher in energy. Therefore, in the temperature range between T^* and ~ 100 K, the spin dynamics are governed by

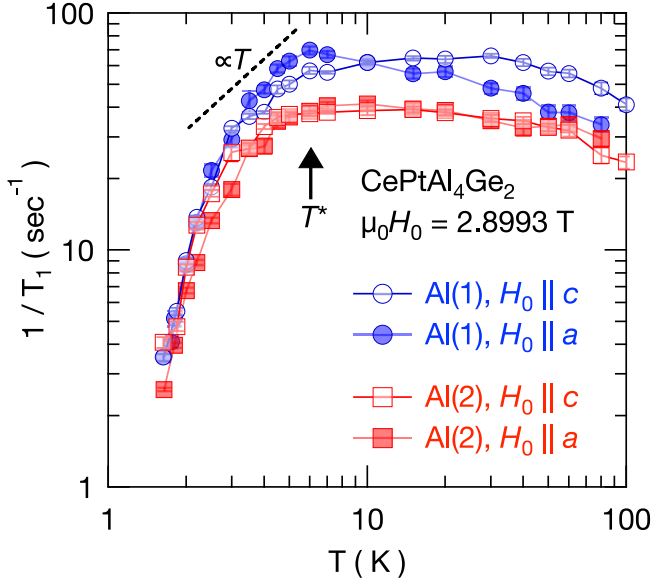


FIG. 4. Temperature dependence of the nuclear spin-lattice relaxation rate $1/T_1$ for the Al(1) and Al(2) sites in $\text{CePtAl}_4\text{Ge}_2$, measured under a magnetic field of $\mu_0 H_0 = 2.8993$ T applied along the a and c axes. The Kondo coherence temperature T^* , as reported by resistivity measurements [12], is indicated by the vertical arrow.

localized moments in the CEF ground state undergoing Kondo interactions with conduction electrons.

In magnetic systems where localized moments are coupled via exchange interactions, Eq. (3) can be simplified to the form proposed by Moriya [25]:

$$\left(\frac{1}{T_1}\right)_{\text{ex}} = \frac{\sqrt{2}\pi (A_{\text{iso}}/z')^2 p_{\text{eff}}^2}{3\hbar^2 \omega_{\text{ex}}}, \quad (4)$$

where the exchange frequency ω_{ex} is given by

$$\omega_{\text{ex}} = \frac{3k_B^2 \theta_W^2}{2z p_{\text{eff}}^2 \hbar^2}. \quad (5)$$

Here, A_{iso} is the isotropic hyperfine coupling constant, z' is the number of magnetic ions surrounding the nuclear site, p_{eff} is the effective magnetic moment, z is the number of nearest-neighbor magnetic ions per Ce site, and θ_W is the Weiss temperature. By substituting $p_{\text{eff}} \approx 1.8 \mu_B$ estimated from the moment of the CEF ground state, and using $\theta_W \approx 2.8$ K from Curie-Weiss fits for $H \parallel c$ in the low temperature range [13], the exchange frequency ω_{ex} can be estimated. For the Al(1) and Al(2) sites, we adopt $|A_{\text{iso}}| = 67$ mT/ μ_B and 85 mT/ μ_B , with $z' = 3$ and 4, respectively. These values yield exchange-narrowed spin-lattice relaxation rates of $(1/T_1)_{\text{ex}} \approx 43$ sec $^{-1}$ for Al(1) and ≈ 39 sec $^{-1}$ for Al(2). The close agreement between these estimates and the experimental $1/T_1$ values supports the applicability of the CEF ground-state configuration proposed in Ref. 13 to the present system.

Upon the formation of Kondo lattice coherence, localized $4f$ moments are expected to evolve into itinerant f electrons, leading to a Korringa-like behavior, i.e.,

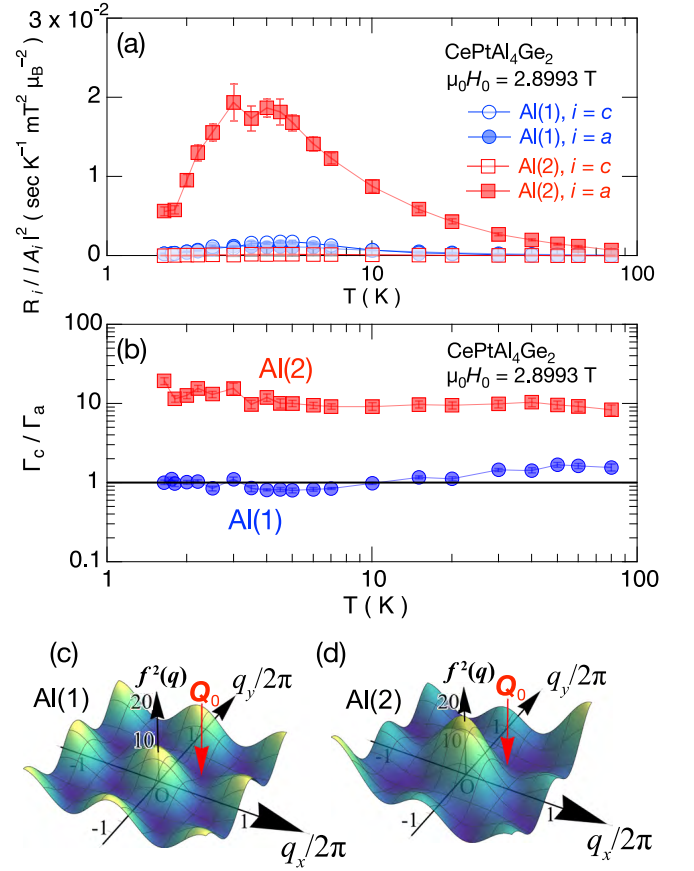


FIG. 5. (a) Temperature dependence of the fluctuation amplitude $R_i/|A_i|^2$ ($i = a, c$) at the Al(1) and Al(2) sites. (b) Temperature dependence of the anisotropy ratio Γ_c/Γ_a for spin fluctuations at each Al site. The quantity Γ_i represents the characteristic energy scale of spin fluctuations along the i -axis; see main text for definition. The hyperfine form factor $|f(\mathbf{q})|^2$ for (c) Al(1) and (d) Al(2) sites, respectively, are illustrated in the q_x - q_y plane. Red arrows indicate the specific point at $\mathbf{Q}_0 = (\frac{1}{3}, \frac{1}{3})$.

$1/T_1 \propto T$. However, in $\text{CePtAl}_4\text{Ge}_2$, $1/T_1$ decreases much more steeply below $T^* \approx 6$ K than expected from this conventional Korringa relation. Such a rapid suppression of $1/T_1$ indicates a substantial reduction of low-energy spin fluctuations. Assuming an activated form for the relaxation rate, $1/T_1 \propto \exp(-E_g/k_B T)$, the data yield an activation energy of $E_g/k_B \sim 10$ K. This behavior suggests the opening of a spin gap or pseudogap in the spin excitation spectrum below T^* , which may be associated with partial gapping of the Fermi surface or the onset of short-range magnetic correlations in the coherent Kondo state.

To further investigate the nature of spin fluctuations, their anisotropy is analyzed by decomposing the fluctuation components along different crystallographic directions. The fluctuation rate along the i -axis ($i = a$ or c)

is defined as

$$R_i \equiv \left(\frac{\gamma_n A_i}{\gamma_e \hbar} \right)^2 k_B \sum_{\mathbf{q}} f^2(\mathbf{q}) \frac{\text{Im } \chi_i(\mathbf{q}, \omega_0)}{\omega_0}. \quad (6)$$

From Eq. (3), the quantities R_i can be obtained experimentally as $R_a = \frac{1}{2}(T_1 T)^{-1}_{H_0 \parallel c}$, $R_c = (T_1 T)^{-1}_{H_0 \parallel a} - R_a$. The fluctuation amplitude along the i -axis is then proportional to $R_i/|A_i|^2$. Assuming a Lorentzian form for the dynamical spin susceptibility, $\{\text{Im } \chi_i(\mathbf{q}, \omega_0)\}/\omega_0 = \chi_i(\mathbf{q})/\Gamma_i(\mathbf{q})$, where $\Gamma_i(\mathbf{q})$ is the characteristic energy scale of magnetic fluctuations, the \mathbf{q} -averaged fluctuation energy is defined as $\Gamma_i \equiv [\overline{\Gamma_i^2(\mathbf{q})}]^{1/2}$. Within the strong correlation limit ($2\pi\chi_i(\mathbf{q})\Gamma_i(\mathbf{q}) \sim 1$) [26], and assuming $f^2(\mathbf{q}) = 1$, this reduces to

$$\Gamma_i = k_B^{1/2} (\gamma_e \hbar)^{-1} \left\{ \frac{\gamma_n A_i}{(2\pi R_i)^{1/2}} \right\}. \quad (7)$$

This approximation is generally valid when discussing spin fluctuation anisotropy at a given site [27–29], except in special cases where antiferromagnetic fluctuations are completely filtered out by symmetry at the nuclear site.

Figure 5(a) shows the temperature dependence of the fluctuation amplitude $R_i/|A_i|^2$ for the Al(1) and Al(2) sites. For Al(2), the in-plane (a -axis) component is strongly enhanced relative to the c -axis component, whereas for Al(1) both components remain much smaller in magnitude. Figure 5(b) presents the temperature dependence of the anisotropy ratio Γ_c/Γ_a , which reflects the ratio of the characteristic fluctuation energies along the two directions. For Al(2), $\Gamma_c/\Gamma_a \approx 10$ with little temperature variation, indicating that $4f$ spin fluctuations in this temperature range are predominantly in-plane. In contrast, the overall fluctuation amplitude for Al(1) is significantly smaller than the in-plane component for Al(2), despite both sites probing the same underlying $4f$ spin dynamics. This pronounced disparity arises from the difference in hyperfine form factors $f(\mathbf{q})$ at the two sites, not meaning that the $4f$ spin fluctuations are different on the nuclear site-to-site.

Figures 5(c) and 5(d) show the calculated $f^2(\mathbf{q})$ in the q_x - q_y plane for Al(1) and Al(2). As illustrated in Fig. 1(c), both sites lie above or below a Ce triangle, but Al(1) has two such triangles in the same Ce plane as nearest and next-nearest neighbors, whereas Al(2) has only one next-nearest Ce neighbor in the adjacent layer. This distinct coordination yields different \mathbf{q} -dependent filtering of magnetic fluctuations: for example, $f^2(\mathbf{Q}_0) = 0$ for Al(1) but $f^2(\mathbf{Q}_0) \neq 0$ for Al(2) at $\mathbf{Q}_0 = (\frac{1}{3}, \frac{1}{3})$, and similar contrasts occur at $\mathbf{Q}_1 = (\frac{1}{2}, 0)$ and $\mathbf{Q}_2 = (0, \frac{1}{2})$. Neutron diffraction, however, finds an incommensurate ordering vector with in-plane component $\mathbf{Q}_{\text{AFM}} = (1.39, 0)$, for which $f^2(\mathbf{Q}_{\text{AFM}}) \neq 0$ at both sites. This implies that AFM fluctuations above T_N may initially emerge along high-symmetry \mathbf{Q}_0 , \mathbf{Q}_1 , or \mathbf{Q}_2 as in a localized-moment system, but in the itinerant f -electron case, the ordering vector is also shaped by the \mathbf{k} -dependent Fermi surface.

The combined influence of geometric frustration and itinerancy likely selects the incommensurate \mathbf{Q}_{AFM} over the nominal high-symmetry points.

In summary, ^{27}Al NMR relaxation reveals strongly anisotropic spin fluctuations in $\text{CePtAl}_4\text{Ge}_2$. Al(2) senses pronounced, nearly temperature-independent in-plane fluctuations, whereas Al(1) experiences much weaker ones due to hyperfine form factor filtering. Thus, the dominant low-energy spin dynamics in the paramagnetic state are in-plane $4f$ AFM fluctuations whose momentum structure is strongly shaped by the triangular lattice network of Ce atoms.

D. AFM order in $\text{CePtAl}_4\text{Ge}_2$

As reported in Ref. 13, $\text{CePtAl}_4\text{Ge}_2$ undergoes an incommensurate longitudinal spin-density-wave (SDW) order — i.e., a spin-amplitude-modulated magnetic structure — with propagation vector $\mathbf{k}_{\text{AFM}} \approx (1.39, 0, 0.09)$ at $T_N = 2.3$ K in zero field. Recent neutron diffraction measurements on single crystals have further revealed that, in the low-field region, the magnetic structure adopts a triple- \mathbf{k} configuration [14]. In a triple- \mathbf{k} state, three symmetry-equivalent modulation vectors \mathbf{k}_1 , \mathbf{k}_2 , and \mathbf{k}_3 contribute simultaneously, producing a noncollinear and noncoplanar spin texture that cannot be represented by a single propagation vector. Neutron diffraction under $H_0 \parallel c$ suggests that a field-induced transition occurs, as shown in Fig. 6(a), accompanied by a slight change in the ordering wave vector and an abrupt suppression of the magnetic Bragg intensity [30]. This may indicate a modification of the triple- \mathbf{k} structure toward another amplitude-modulated configuration in the high-field AFM phase. In both the zero-field triple- \mathbf{k} AFM structure and the field-modified AFM state, which are forms of incommensurate longitudinal SDW order, the NMR spectra are expected to broaden significantly because the ^{27}Al nuclei sense both the external field and site-dependent internal hyperfine fields arising from the spatial modulation of Ce moments. As established in Sec. III B, the hyperfine coupling constant at the Al(2) site is larger than that at the Al(1) site, and as shown in Sec. III C, the form factor does not suppress the internal field at relevant \mathbf{q} -vectors. Therefore, the Al(2) site is particularly suitable for probing the AFM state by NMR.

Figure 6(b) shows the ^{27}Al (2) NMR spectra at $\mu_0 H_0 = 1.4985$ T ($\parallel c$), where the system enters the high-field AFM phase at low temperatures, as indicated in Fig. 6(a). Below $T_N(H_0)$, the spectra broaden markedly, and at $T = 0.1$ K they are substantially wider than in the paramagnetic state. The shift of the peak position below $T_N(H_0)$ corresponds to a reduction of the Knight shift, reflecting the decrease in the macroscopic susceptibility upon the onset of AFM order. In such an SDW state, there are always positions where the internal field is canceled, and the spectrum broadens symmetrically around these zero internal field sites. A similar broad-

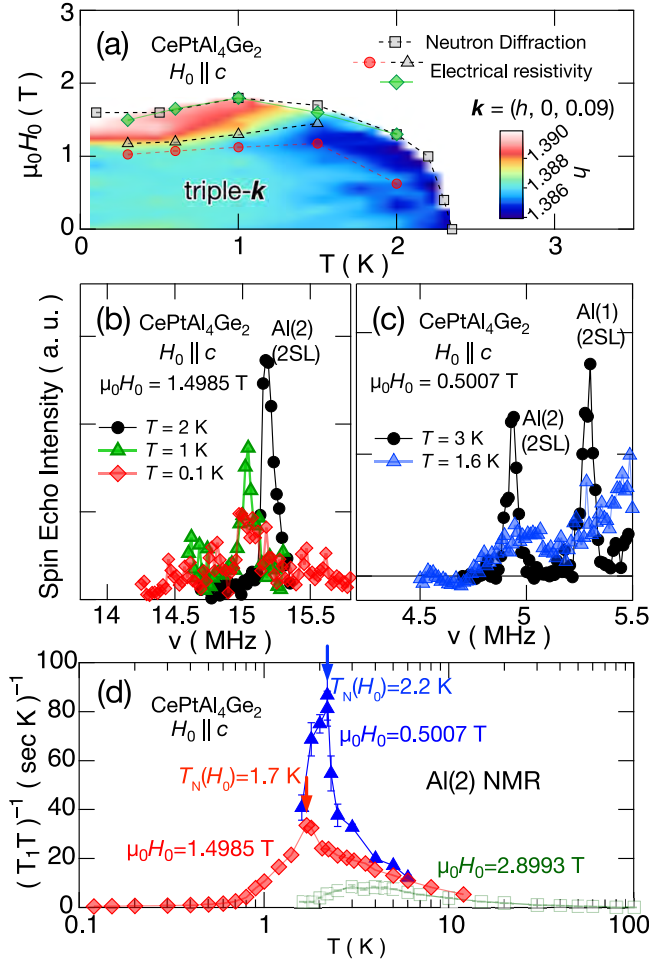


FIG. 6. (a) H_0 - T phase diagram of $\text{CePtAl}_4\text{Ge}_2$ for $H_0 \parallel c$, determined from neutron diffraction and electrical resistivity measurements [30]. The color contour represents the h -index of the incommensurate ordering vector $\mathbf{k} = (h, 0, 0.09)$. (b) ^{27}Al NMR spectra of the lower-frequency-side second satellite (2SL) transition of the Al(2) sites under $\mu_0 H_0 = 1.4985$ T. (c) ^{27}Al NMR spectra of the 2SL transition of the Al(1) and Al(2) sites under $\mu_0 H_0 = 0.5007$ T. (d) Temperature dependence of $(T_1 T)^{-1}$ at the Al(1) and Al(2) sites, measured under $\mu_0 H_0 = 0.5007, 1.4985$, and 2.8993 T with $H_0 \parallel c$. Vertical arrows indicate the Néel temperatures $T_N(H_0)$ at each field.

ening is observed at $\mu_0 H_0 = 0.5007$ T [Fig. 6(c)], although no reliable spectra could be obtained below 1.6 K. This loss of signal likely originates from the combined effects of reduced NMR signal intensity at low fields and pronounced line broadening associated with the triple- \mathbf{k} structure. The inability to detect signals below 1.6 K in low fields suggests that the sensitivity of the present ^3He - ^4He dilution-refrigerator NMR setup was insufficient for such conditions. As demonstrated in the detailed NMR study of the polar magnet GaV_4Se_8 hosting a Néel-type skyrmion lattice [31], future investigations of the triple- \mathbf{k} structure will require larger single crystals and improved probe sensitivity.

The $1/T_1$ results for various fields are summarized in

Fig. 6(d). At $\mu_0 H_0 \approx 2.9$ T, $(T_1 T)^{-1}$ shows a broad maximum at 3–4 K, below T^* , indicative of a pseudogap-like suppression of spin fluctuations. At $\mu_0 H_0 \approx 1.5$ T, $(T_1 T)^{-1}$ increases continuously toward $T_N(H_0)$. Further lowering the field to $\mu_0 H_0 \approx 0.5$ T leads to a more pronounced enhancement of $(T_1 T)^{-1}$ on cooling, signaling the growth of in-plane spin fluctuations approaching the AFM transition. Below $T_N(H_0)$, $(T_1 T)^{-1}$ drops sharply, marking the onset of long-range magnetic order, and the transition temperatures agree well with those in the H_0 - T phase diagram of Fig. 6(a).

IV. CONCLUSION

A comprehensive site-selective ^{27}Al NMR investigation has been carried out on the triangular Kondo lattice compound $\text{CePtAl}_4\text{Ge}_2$, which exhibits incommensurate antiferromagnetic order below $T_N = 2.3$ K. The two inequivalent Al sites were unambiguously assigned through comparisons of experimental quadrupolar parameters with the calculated EFG from the electronic structure calculation, enabling the determination of site-resolved hyperfine coupling constants. These results show that the magnetic couplings are dominated by transferred RKKY-type interactions rather than simple dipolar fields. In the paramagnetic state, $1/T_1$ measurements revealed pronounced anisotropic spin fluctuations with a predominantly in-plane character. Below the Kondo coherence temperature $T^* \approx 6$ K, $1/T_1$ decreases much more steeply than expected from Korringa behavior, suggesting the opening of a spin gap of order ~ 10 K as the Ce $4f$ moments evolve into a coherent heavy Fermi liquid. Comparison of fluctuation amplitudes at the two Al sites demonstrated that the apparent site dependence originates from the distinct hyperfine form factors $f(\mathbf{q})$. The incommensurate ordering vector \mathbf{Q}_{AFM} determined by neutron diffraction yields finite $f^2(\mathbf{Q}_{\text{AFM}})$ at both sites, indicating that long-range order develops at a geometrically compromised wave vector selected from underlying frustrated correlations.

In the ordered state, NMR spectra broaden substantially and $(T_1 T)^{-1}$ drops sharply below $T_N(H_0)$, consistent with the onset of long-range magnetic order. The magnetic-field dependence of $(T_1 T)^{-1}$ reveals that in-plane spin fluctuations are strongly enhanced near T_N , particularly at low fields.

These findings establish $\text{CePtAl}_4\text{Ge}_2$ as a clean platform for studying frustrated Kondo magnetism in a triangular lattice network, and demonstrate the effectiveness of site-selective NMR in resolving momentum-dependent spin dynamics and complex spin textures in correlated f -electron systems. The predominance of in-plane spin fluctuations found here bears a notable resemblance to that observed in the triangular Kondo lattice compound YbV_6Sn_6 , suggesting a common underlying mechanism arising from the synergy of Kondo physics and geometrical frustration in layered f -electron materials [32]. Taken

together, our results on $\text{CePtAl}_4\text{Ge}_2$ provide microscopic insight into how geometric frustration and Kondo coherence intertwine to shape unconventional magnetism in f -electron systems.

ACKNOWLEDGMENTS

We thank T. Kitazawa and Y. Haga for their assistance with single-crystal orientation and for fruitful dis-

cussions. This work was supported by Japan Society for the Promotion of Science (JSPS) through KAKENHI (JP23K25829, JP24KK0062, and JP24K00587). Work at the Japan Atomic Energy Agency (JAEA) was partially supported by the JAEA REIMEI Research Program. S. S. acknowledges support from the Swiss National Science Foundation SNSF Project No. 200021_188706. Work at Sungkyunkwan University was supported by the National Research Foundation (NRF) of Korea through a grant funded by the Korean government (No. RS-2023-00220471 and RS-2021-NR059409).

-
- [1] Q. Si, Global magnetic phase diagram and local quantum criticality in heavy fermion metals, *Physica B: Condensed Matter* **378-380**, 23 (2006).
 - [2] M. Vojta, From itinerant to local-moment antiferromagnetism in kondo lattices: Adiabatic continuity versus quantum phase transitions, *Phys. Rev. B* **78**, 125109 (2008).
 - [3] P. Coleman and A. H. Nevidomskyy, Frustration and the kondo effect in heavy fermion materials, *Journal of Low Temperature Physics* **161**, 182 (2010).
 - [4] C. D. Batista, S.-Z. Lin, S. Hayami, and Y. Kamiya, Frustration and chiral orderings in correlated electron systems, *Reports on Progress in Physics* **79**, 084504 (2016).
 - [5] A. Dönni, G. Ehlers, H. Maletta, P. Fischer, H. Kitazawa, and M. Zolliker, Geometrically frustrated magnetic structures of the heavy-fermion compound CePdAl studied by powder neutron diffraction, *Journal of Physics: Condensed Matter* **8**, 11213 (1996).
 - [6] A. Oyamada, S. Maegawa, M. Nishiyama, H. Kitazawa, and Y. Isikawa, Ordering mechanism and spin fluctuations in a geometrically frustrated heavy-fermion antiferromagnet on the kagome-like lattice CePdAl : A ^{27}Al NMR study, *Phys. Rev. B* **77**, 064432 (2008).
 - [7] H. Zhao, J. Zhang, S. Hu, Y. Isikawa, J. Luo, F. Steglich, and P. Sun, Temperature-field phase diagram of geometrically frustrated CePdAl , *Phys. Rev. B* **94**, 235131 (2016).
 - [8] S. Lucas, K. Grube, C.-L. Huang, A. Sakai, S. Wunderlich, E. L. Green, J. Wosnitza, V. Fritsch, P. Gegenwart, O. Stockert, and H. v. Löhneysen, Entropy evolution in the magnetic phases of partially frustrated CePdAl , *Phys. Rev. Lett.* **118**, 107204 (2017).
 - [9] S. A. M. Mentink, A. Drost, G. J. Nieuwenhuys, E. Frikkie, A. A. Menovsky, and J. A. Mydosh, Magnetic ordering and frustration in hexagonal UNi_4B , *Phys. Rev. Lett.* **73**, 1031 (1994).
 - [10] S. A. M. Mentink, G. J. Nieuwenhuys, H. Nakotte, A. A. Menovsky, A. Drost, E. Frikkie, and J. A. Mydosh, Magnetization and resistivity of UNi_4B in high magnetic fields, *Phys. Rev. B* **51**, 11567 (1995).
 - [11] R. Movshovich, M. Jaime, S. Mentink, A. A. Menovsky, and J. A. Mydosh, Second low-temperature phase transition in frustrated UNi_4B , *Phys. Rev. Lett.* **83**, 2065 (1999).
 - [12] S. Shin, P. F. Rosa, F. Ronning, J. D. Thompson, B. L. Scott, S. Lee, H. Jang, S.-G. Jung, E. Yun, H. Lee, E. D. Bauer, and T. Park, Synthesis and characterization of the heavy-fermion compound $\text{CePtAl}_4\text{Ge}_2$, *Journal of Alloys and Compounds* **738**, 550 (2018).
 - [13] S. Shin, V. Pomjakushin, L. Keller, P. F. S. Rosa, U. Stühr, C. Niedermayer, R. Sibille, S. Toth, J. Kim, H. Jang, S.-K. Son, H.-O. Lee, T. Shang, M. Medarde, E. D. Bauer, M. Kenzelmann, and T. Park, Magnetic structure and crystalline electric field effects in the triangular antiferromagnet $\text{CePtAl}_4\text{Ge}_2$, *Phys. Rev. B* **101**, 224421 (2020).
 - [14] S. Shin, J.-H. Park, R. Sibille, H. Jang, T. B. Park, S. Kim, T. Shang, M. Medarde, E. D. Bauer, O. Zaharko, M. Kenzelmann, and T. Park, Triple-sinusoid hedgehog lattice in a centrosymmetric kondo metal (2023), arXiv:2311.13405 [cond-mat.str-el].
 - [15] N. J. Ghimire, F. Ronning, D. J. Williams, B. L. Scott, Y. Luo, J. D. Thompson, and E. D. Bauer, Investigation of the physical properties of the tetragonal $\text{CeMAl}_4\text{Si}_2$ ($M = \text{Rh, Ir, Pt}$) compounds, *J. Phys.: Condens. Matter* **27**, 025601 (2015).
 - [16] A. Maurya, R. Kulkarni, A. Thamizhavel, D. Paudyal, and S. K. Dhar, Kondo lattice and antiferromagnetic behavior in quaternary $\text{CeTAl}_4\text{Si}_2$ ($T = \text{Rh, Ir}$) single crystals, *Journal of the Physical Society of Japan* **85**, 034720 (2016).
 - [17] H. Sakai, T. Hattori, Y. Tokunaga, S. Kambe, N. J. Ghimire, F. Ronning, E. D. Bauer, and J. D. Thompson, Incommensurate to commensurate antiferromagnetism in $\text{CeRhAl}_4\text{Si}_2$: An ^{27}Al NMR study, *Phys. Rev. B* **93**, 014402 (2016).
 - [18] P. Pykkö, Year-2008 nuclear quadrupole moments, *Molecular Physics* **106**, 1965 (2008).
 - [19] P. Blaha, D. J. Singh, P. I. Sorantin, and K. Schwarz, Electric-field-gradient calculations for systems with large extended-core-state contributions, *Phys. Rev. B* **46**, 1321 (1992).
 - [20] M. Matsumura, Y. Kawamura, S. Edamoto, T. Takesaka, H. Kato, T. Nishioka, Y. Tokunaga, S. Kambe, and H. Yasuoka, Novel phase transition in $\text{CeRu}_2\text{Al}_{10}$ probed by ^{27}Al -NQR/NMR –no evidence of magnetic ordering–, *Journal of the Physical Society of Japan* **78**, 123713 (2009).
 - [21] H. Matsuno, H. Nohara, H. Kotegawa, E. Matsuoka, Y. Tomiyama, H. Sugawara, H. Harima, and H. Tou, Ising-type magnetic anisotropy derived by $\Gamma_7^{(2)}$ crystal electric field ground state in tetragonal $\text{CeRu}_2\text{Al}_2\text{B}$: ^{11}B and ^{27}Al NMR studies, *J. Phys. Soc. Jpn.* **81**, 073705 (2012).
 - [22] H. Sakai, Y. Tokunaga, S. Kambe, R. E. Baumbach,

- F. Ronning, E. D. Bauer, and J. D. Thompson, NMR study for 4f-localized ferromagnet $\text{CeRu}_2\text{Ga}_2\text{B}$, *Phys. Rev. B* **86**, 094402 (2012).
- [23] T. C. Kobayashi, K. Fujiwara, K. Takeda, H. Harima, Y. Ikeda, T. Adachi, Y. Ohishi, C. Geibel, and F. Steglich, Valence crossover of Ce ions in CeCu_2Si_2 under high pressure –pressure dependence of the unit cell volume and the NQR frequency–, *J. Phys. Soc. Jpn.* **82**, 114701 (2013).
- [24] T. Moriya, The effect of electron-electron interaction on the nuclear spin relaxation in metals, *J. Phys. Soc. Jpn.* **18**, 516 (1963).
- [25] T. Moriya, Nuclear magnetic relaxation in antiferromagnetics, I, II, *Prog. Theor. Phys.* **16**, 23,641 (1956).
- [26] T. Moriya and T. Takimoto, Anomalous properties around magnetic instability in heavy electron systems, *J. Phys. Soc. Jpn.* **64**, 960 (1995).
- [27] S. Kambe, H. Sakai, Y. Tokunaga, T. Fujimoto, R. E. Walstedt, S. Ikeda, D. Aoki, Y. Homma, Y. Haga, Y. Shiokawa, and Y. Ōnuki, Favorable magnetic fluctuation anisotropy for unconventional superconductivity in f -electron systems, *Phys. Rev. B* **75**, 140509(R) (4) (2007).
- [28] H. Sakai, S.-H. Baek, S. E. Brown, F. Ronning, E. D. Bauer, and J. D. Thompson, ^{59}Co NMR shift anomalies and spin dynamics in the normal state of superconducting CeCoIn_5 : Verification of two-dimensional antiferromagnetic spin fluctuations, *Phys. Rev. B* **82**, 020501(R) (2010).
- [29] S.-H. Baek, H. Sakai, E. D. Bauer, J. N. Mitchell, J. A. Kennison, F. Ronning, and J. D. Thompson, Anisotropic spin fluctuations and superconductivity in “115” heavy fermion compounds: ^{59}Co NMR study in PuCoGa_5 , *Phys. Rev. Lett.* **105**, 217002 (2010).
- [30] S. Shin et al., H - T phase diagram of $\text{CePtAl}_4\text{Ge}_2$ for $H \parallel c$, in preparation.
- [31] H. Takeda, M. Ishikawa, M. Takigawa, M. Yamashita, Y. Fujima, and T.-h. Arima, Magnetic structure of polar magnet GaV_4Se_8 with Néel-type skyrmion lattice probed by ^{51}V NMR, *Phys. Rev. B* **110**, 224430 (2024).
- [32] S. Park, H. Sakai, S. Hosoi, S. M. Thomas, S. Kambe, Y. Tokunaga, A. P. Dioguardi, J. D. Thompson, F. Ronning, M. Kimata, T. Furukawa, T. Sasaki, E. D. Bauer, and M. Hirata, Investigation of the paramagnetic state of the kagome kondo lattice compound YbV_6Sn_6 : a ^{51}V nuclear magnetic resonance study (2025), arXiv:2506.04563 [cond-mat.str-el].